



# Low temperature edge dynamics of AB-stacked bilayer graphene: Naturally favored closed zigzag edges

Da Zhan<sup>1</sup>, Lei Liu<sup>1,4</sup>, Ya Nan Xu<sup>1,2</sup>, Zhen Hua Ni<sup>3</sup>, Jia Xu Yan<sup>1</sup>, Chun Zhao<sup>2</sup> & Ze Xiang Shen<sup>1</sup>

<sup>1</sup>Division of Physics and Applied Physics, School of Physical and Mathematical Sciences, Nanyang Technological University, 637371 Singapore, <sup>2</sup>State Key Laboratory on Integrated Optoelectronics, College of Electronic Science and Engineering, Jilin University, 2699 Qianjin Street, Changchun, 130012 China, <sup>3</sup>Department of Physics, Southeast University, Nanjing, 211189 China, <sup>4</sup>Key Laboratory of Excited State Processes, Changchun Institute of Optics, Fine Mechanics and Physics (CIOMP), Changchun, 130033 China.

Received  
28 January 2011

Accepted  
14 April 2011

Published  
14 June 2011

Correspondence and requests for materials should be addressed to Z.X.S. (zexiang@ntu.edu.sg)

Closed edges bilayer graphene (CEBG) is a recent discovered novel form of graphene structures, whose regulated edge states may critically change the overall electronic behaviors. If stacked properly with the AB style, the bilayer graphene with closed zigzag edges may even present amazing electronic properties of bandgap opening and charge separation. Experimentally, the CEBG has been confirmed recently with HRTEM observations after extremely high temperature annealing (2000 °C). From the application point of view, the low temperature closing of the graphene edges would be much more feasible for large-scale graphene-based electronic devices fabrication. Here, we demonstrate that the zigzag edges of AB-stacked bilayer graphene will form curved close structure naturally at low annealing temperature (< 500 °C) based on Raman observation and first principles analysis. Such findings may illuminate a simple and easy way to engineer graphene electronics.

The electronic and transport properties of graphene are strongly dependent on its edge structures<sup>1</sup>, and therefore graphene with edges, so called graphene nanoribbons (GNRs), have been intensively studied<sup>2–15</sup> since its experimental isolation. As the crucial step for fabricating graphene into future nanoelectronics<sup>2,16,17</sup>, understanding the thermal dynamics of its edges has been the major focus among those studies. Recently, we revealed that the zigzag edge (Z-edge) of single layer graphene (SLG) is thermally unstable and they can be easily modified to form armchair segments along  $\pm 30^\circ$  with respect to the original edge direction<sup>16</sup>. For bilayer graphene (BLG), Liu *et al.* observed by HRTEM<sup>2</sup> that BLGs would transform to AA-stacked style with closed edges after extremely high temperature annealing (2000 °C). Meanwhile, using NEXFAS<sup>17</sup>, Joly *et al.* indirectly observed the loop formation of the edges of few-layer graphene (FLG) after high temperature annealing (1500–2000 °C). However, the information about low temperature thermal dynamic behavior of AB-stacked BLG is still very limited. For example, few reports notice the rule that, for AB-stacked BLG under low temperature which impeded layer gliding, geometry incompatibility limit armchair edges (A-edges) form closing edges with perfect sp<sup>2</sup> hybridized C-C bonds (Fig. 1c,d), and allow only zigzag edges (Z-edges) form closed edge loop (Fig. 1a,b). Therefore, AB-stacked CEBG with Z-edges could be formed under low temperature. Furthermore, our recent theoretical work predicted that the AB-stacked CEBG will present the unusual electronic properties of band gap opening and charges separation due to pseudospin repulsion<sup>4</sup> makes detailed experimental observation on the CEBG edges fundamentally meaningful. While AB stacking is the native stacking style of graphene layers<sup>18</sup> and low temperature processing of graphene is also much more practically desirable, further investigation on low temperature thermal dynamic behaviors of AB-stacked BLG edges would be timely and meaningful towards the complete understanding of BLG edge dynamics.

In this paper, we using Density Functional Theory (DFT) calculation theoretically predict that the AB-stacked CEBG can be formed easily because of the energetically favorable. Polarized Raman spectroscopy and Raman images were carried out to investigate the thermal dynamics of AB-stacked FLG edges, and the experimental results provide clear evidence that the AB-stacked CEBG can be formed at very low temperature (<500 °C).

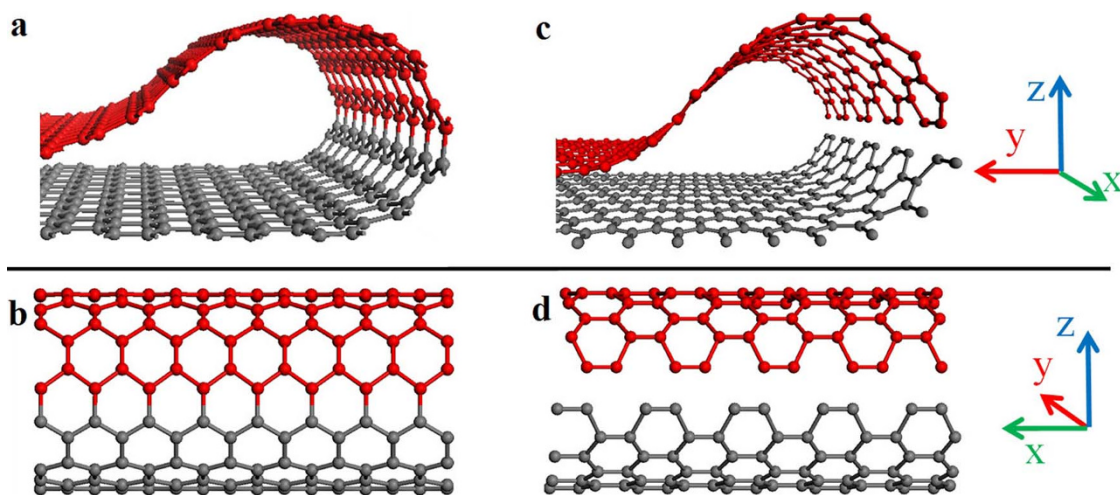


**Figure 1** | Schematic atomic structure for AB-stacked BLG edges. (a,b) Geometrically compatible closed Z-edges; (c,d) Geometrically incompatible that A-edges cannot form closed structure.

## Results

The formation of AB-stacked CEBG can be understood by DFT calculation results. Figure 2 shows the evolution of system energy for AB-stacked BLG from its initial open edge to the final relaxed state with closed Z-edges through a dynamic process. In this

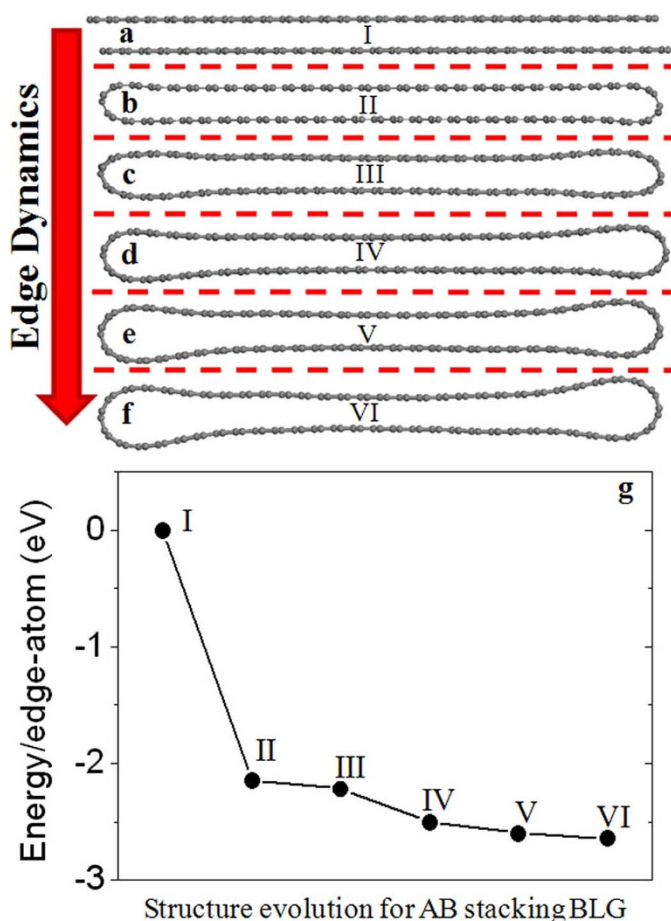


**Figure 2** | Modeling of the closed Z-edges of BLG formation from the initial open-edge configuration. (a,b) Edge structure evolution from open edges to closed edges; (c–f) The energy relaxation dynamics of closed edges by curvature smoothing. (g) The system energy evolution versus the modeled structure configurations as shown in (a–f).

simulation study, we did not observe any energy barrier from the initial open edge state to closed edge state, instead, the system energy undergoes more than 2 eV drop when the atoms on the top and bottom Z-edges firstly bonded. Afterward, the system energy further decreases slightly (Fig. 2g) by structure relaxing (Fig. 2b–f). Therefore, it is clear that the AB-stacked CEBG is dynamically and energetically favorable. Furthermore, it is also reported that the open and sharp Z-edges of AB-stacked BLG can be transformed to CEBG rapidly according to the quantum molecular dynamics simulation results<sup>19</sup>.

To confirm this theoretical prediction, we carried out systematic experimental studies based on Raman spectroscopy. Raman spectroscopy is a non-destructive, fast and effective tool for investigating graphene-based material<sup>20</sup>, not only for detecting defects, doping and intercalation<sup>21–24</sup> but also for identifying edge structures<sup>11,12,14,16</sup>; the D band is inactive for Z-edge but it is activated for A-edge, and its intensity is strongly dependent on incident laser polarization. Figure 3a–c show the integrated G peak Raman images of graphene flakes with layer number of 1 (SLG), 2 (BLG) and 3 (Trilayer graphene, TLG), respectively (both BLG and TLG have AB stacking sequence). Each graphene sample consists of two sharp edges with angle of 150°, meaning that two edges must have different chiralities. Figure 3d–f show Raman images of D peak intensity for pristine graphene samples of SLG, BLG, and TLG, respectively. A prominent D peak observed along the left edge (edge A<sub>1</sub>, B<sub>1</sub>, and C<sub>1</sub>) of each sample indicates a predominantly armchair edge, while the absence of obvious D peak for the right edge for each sample (edge A<sub>2</sub>, B<sub>2</sub>, and C<sub>2</sub>) indicates a predominantly zigzag edge<sup>11,12,14,25</sup>. Raman images of the D peak intensity of the same samples after 500 °C annealing are shown in Figure 3g–i. It is noticed that there is no obvious change in the D peak intensity for annealed A-edges (left edges) of each sample as they still show prominent D peak. Furthermore, for Raman spectra of A-edges of SLG, BLG and TLG (Fig. 4c,d), the intensity ratio of I<sub>D</sub>/I<sub>G</sub> decreases slightly after anneal, because annealing induced doping results in a decrease in the D peak intensity<sup>26</sup>. The results of Raman images and spectra indicate that thermal dynamic behavior for few-layer graphene (BLG and TLG) A-edges is similar to that of SLG<sup>16</sup>, and we will show detailed analysis of the annealed A-edges by polarized Raman results later.

On the other hand, for Z-edges, SLG and TLG respectively show strong D peak after annealing, while the D peak of BLG almost keeps Raman inactive after annealing. Raman spectra for pristine and annealed Z-edges are respectively shown in Figure 4a,b. It is clearly seen that only Z-edges of SLG and TLG show prominent D peak after annealing while the BLG still shows absence of the D peak similar to

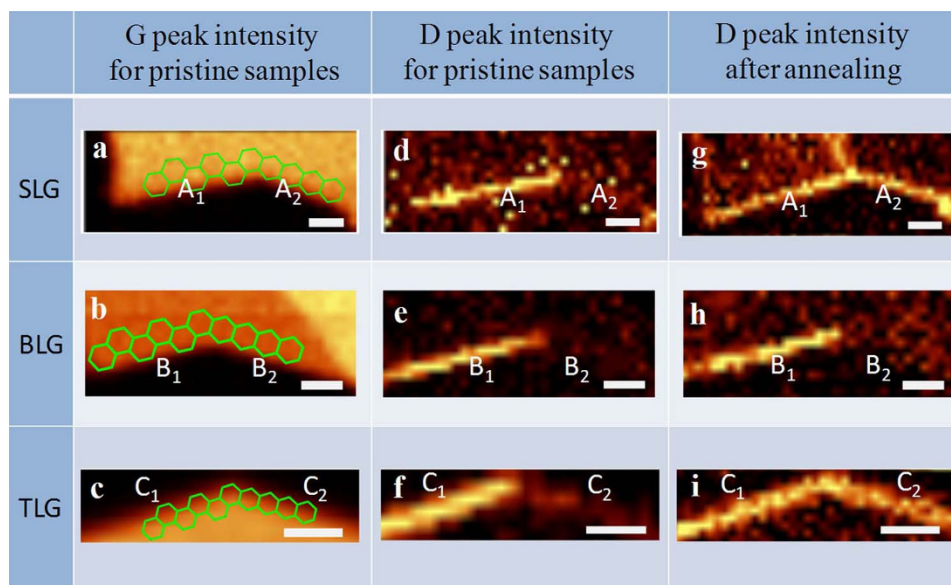


**Figure 3 | Raman images for SLG, BLG and TLG.** (a–c) G peak intensity for pristine SLG, BLG and TLG, respectively; (d–f) D peak intensity for pristine SLG, BLG and TLG; (g–i) D peak intensity for annealed SLG, BLG and TLG. The polarizations of the incident laser are all horizontal and the scale bar for each image is 1  $\mu\text{m}$ .

that of precursor pristine sample. We have examined more than 20 Z-edges and all SLGs and TLGs show obvious activated D peak after annealing while the BLGs do not. The behavior of SLG can be easily understood as thermal dynamics of Z-edges of SLG has been reported elsewhere by our group<sup>16</sup>. It has been revealed that Z-edges of SLG are not thermally stable and can be easily transformed to armchair segments at  $\pm 30^\circ$  with respect to the original edge

direction after annealing, and thus it presents strong D peak<sup>16</sup>. However, the behavior of BLG after annealing is very different. One reasonable explanation for BLG Z-edges is that the low temperature annealing leads the carbon atoms of top and bottom edges bond to each other to form intact  $\text{sp}^2$  hybridized smooth loop configuration, which follows our simulation results (Fig. 2). As there are no open edges, it is reasonable to expect the D band remains absent when the loop is smooth enough<sup>27</sup>.

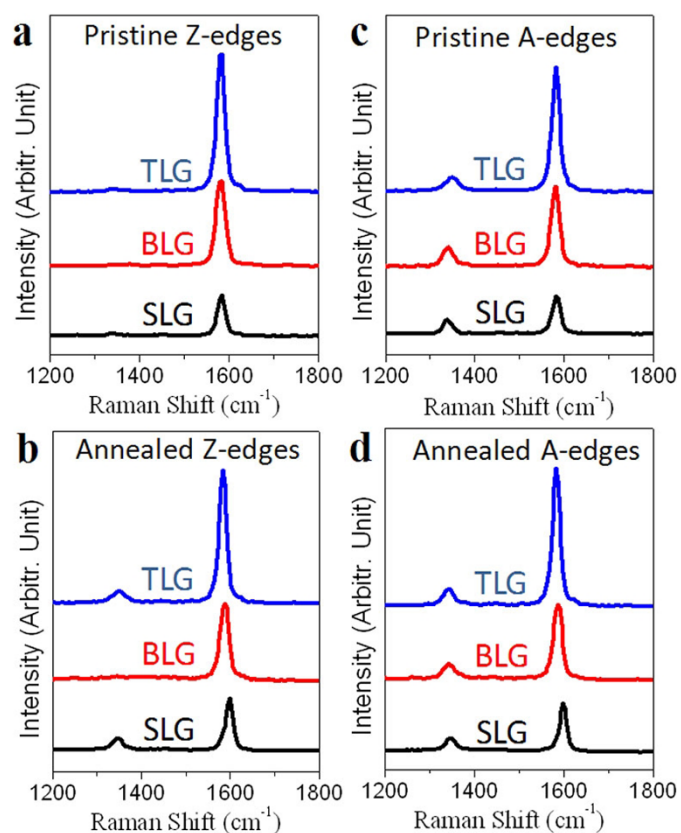


**Figure 4 | Raman spectra for SLG, BLG and TLG.** Pristine (a) and annealed (b) Z-edges; Pristine (c) and annealed (d) A-edges.

Because D peak intensity is strongly dependent on laser polarization for armchair segments, we carried out polarized Raman study to further analyze the thermal dynamic behavior of A-edges and Z-edges in details. Figure 5 shows the experimentally obtained  $I_D/I_G$  as function of  $\theta$  for pristine and annealed edges (SLG, BLG and TLG).  $\theta$  is the angle between incident laser polarization and edge direction; for each  $\theta$ , line scan was used to determine the exact edge position by observing maximum D peak intensity  $I_D$ . The fitted curves for A-edges and Z-edges are based on the formulas described in Ref. [16] throughout this paper. For annealed Z-edges, BLG only shows very weak  $I_D/I_G$  even when the incident laser polarization is parallel to the edge direction; while TLG not only shows obvious activated D peak similar to that of SLG, but the polarization dependent tendency is also very similar. For SLG, a large portion of the Z-edge is easily modified in form of armchair segments at  $\pm 30^\circ$  after 500  $^\circ\text{C}$  annealing, and hence  $I_D/I_G$  shows some extent polarization dependence<sup>16</sup>. Based on above results, we conclude that for TLG, although two of the adjacent open Z-edges may form closed structure, the D peak must be activated because at least one lonely Z-edge of TLG should follow similar structure modification as that of SLG upon annealing<sup>16</sup>.

For A-edges, the pristine SLG, BLG and TLG present obvious polarization dependent intensity ratio of  $I_D/I_G$  (Fig. 5a–c). After annealing, the polarization dependent intensity ratio of  $I_D/I_G$  becomes slightly weaker (Fig. 5d–f). For SLG, the weaker polarization dependence of A-edge is explained as the edge structure modification (*i.e.* Some portion transforms to armchair segments at  $\pm 60^\circ$  with respect to the original edge direction and hence weaken the total polarization dependence)<sup>16</sup>. The similar dependent tendency of polarized intensity ratio of  $I_D/I_G$  for TLG and BLG to that of SLG indicates that the A-edges of TLG and BLG have similar thermal dynamic behavior as that of SLG. In other words, the A-edges of

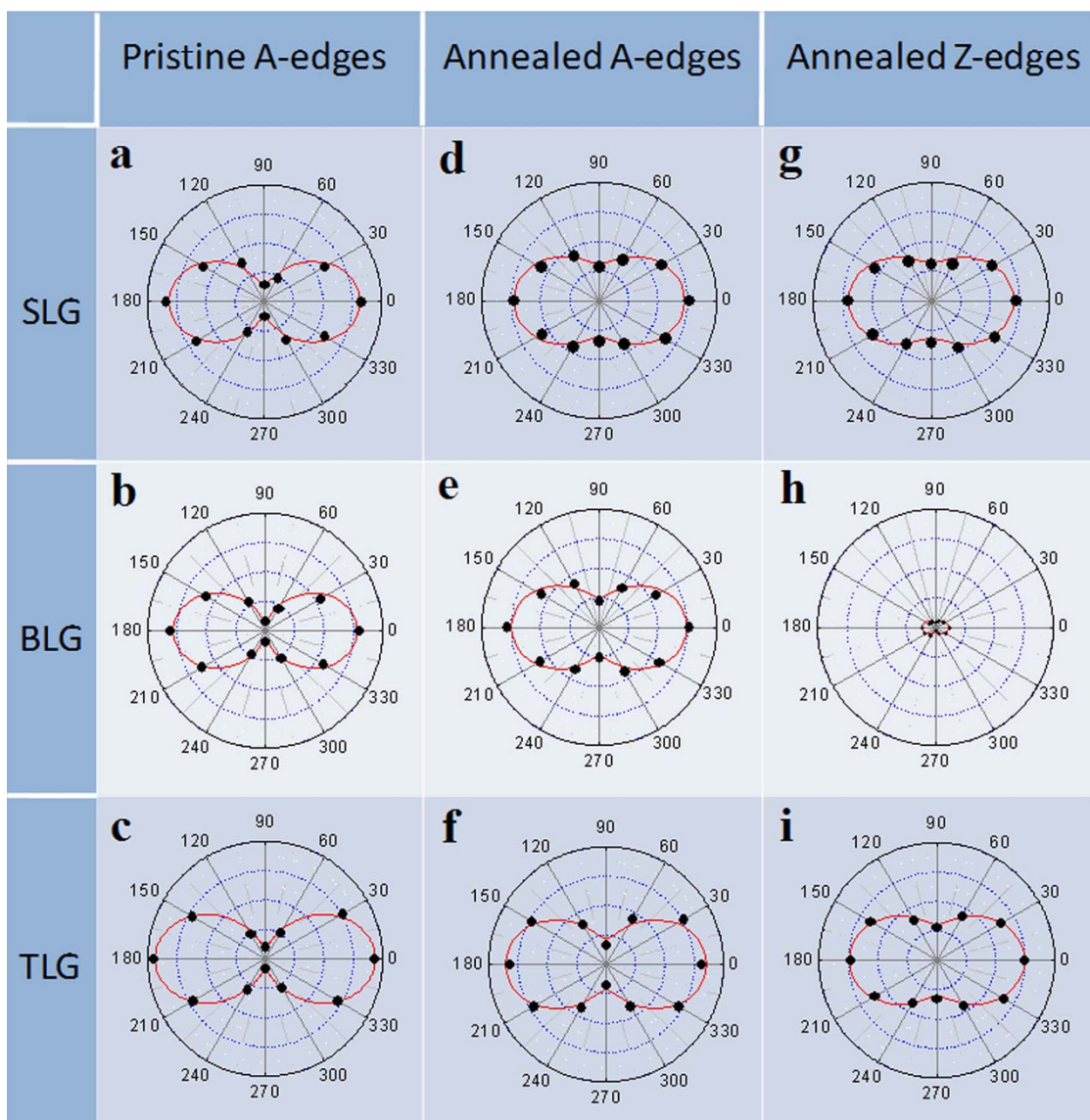


**Figure 5 | Polarization dependence of  $I_D/I_G$  for SLG, BLG and TLG.**  $\theta$  is the angle between laser polarization and edge direction. (a–c) Pristine A-edges for SLG, BLG and TLG, respectively. (d–f), Annealed A-edges for SLG, BLG and TLG, respectively. (g–i) Annealed Z-edges for SLG, BLG and TLG, respectively. The scale bar for the polar graphs is 0–0.5 for SLG, 0–0.35 for BLG and 0–0.2 for TLG.

TLG and BLG can be respectively considered as three and two independent individual A-edges when they are undergone thermal treatment. This is reasonable because unlike Z-edges which can form closed structure upon annealing, the adjacent A-edges of AB-stacked FLG cannot form perfect  $sp^2$  hybridized closed structure due to geometrical incompatibility as aforementioned (Fig. 1c,d).

## Discussion

Liu *et al.* recently reported that AB-stacked graphite transformed to AA-stacked BLGs with both A-edges and Z-edges closed after extremely high temperature annealing (2000 °C)<sup>2</sup>. Here, we propose a thermal dynamic model to elucidate the structure evolution for AB-stacked BLG edges (both Z-edges and A-edges) according to our low temperature experimental results and high temperature results elsewhere<sup>2</sup>: When AB-stacked BLG annealed at low temperature, Z-edges start to form closed structure because such edge structure is geometrically compatible and energetically favorable (Fig. 1a,b and Fig. 2), while the A-edges keep open because of geometrical incompatibility for the formation of closed structure (Fig. 1c,d). When the temperature increases, the thermal vibrating amplitude

of carbon atoms becomes much larger (Fig. 1a,b). When the annealing temperature is high enough (*i.e.*  $\sim 2000$  °C), the top and bottom graphene layers have very high opportunity to transform to AA stacking sequence which requires a shift of the graphene layer by a C–C bond length along the x-axis (Fig. 1d). In that case, atoms on the A-edges can bond each other to form interconnected configuration similar to Z-edges<sup>28</sup>. This thermal dynamic model for the edge structure evolution explains the results that AB-stacked graphite transforms to AA-stacked BLGs with both closed Z-edges and A-edges<sup>2</sup>.

In conclusion, we revealed by DFT calculations and systematic Raman investigations that the AB-stacked open Z-edges of BLG can transform to closed  $sp^2$  hybridized structure easily even at very low annealing temperature because such structure is geometrically compatible and energetically favorable, and the closed edges are thermally stable. In contrast to thermal dynamic behavior of Z-edges, A-edges of AB-stacked BLG cannot form closed  $sp^2$  hybridized structure due to geometrical incompatibility, and thus the A-edges for BLG behaves as two independent SLGs. The formation of closed Z-edges for AB-stacked BLG by low temperature treatment matches the semiconductor manufacturing process, thus this finding may



benefit graphene-based nanoelectronics as closed edges of AB-stacked BLG is predicted to present exotic electronic properties, such as pseudospin repulsion induced bandgap opening and charge separation<sup>4</sup>.

## Methods

**Fabrication of pristine and annealed SLG, BLG and TLG.** Graphene samples were prepared by conventional micromechanical cleavage method on silicon wafer covered by 300 nm SiO<sub>2</sub>. The layer number from 1L to 3L of graphene flakes were confirmed by Raman and contrast spectra<sup>29–31</sup>.

**Raman spectroscopy measurements.** The Raman spectra were carried out with a WITTEC CRM200 Raman system, with excitation laser wavelength of 532 nm and 100× objective lens (Numerical Aperture, NA=0.95). The laser power at sample is below 1 mW to avoid possible laser heating induced sample damage<sup>32</sup>. Raman images with a spatial resolution of ~600 nm are realized with a piezo stage (step size 100 nm) and the integration time at each position is one second. Samples with straight edges and angle of 150° between adjacent edges were selected so that for each sample, one edge is A-edges (strong D peak) and the other is Z-edges (weak D peak). Each single Raman spectrum of graphene edges is determined by Raman line scan (step size 50 nm) across the edge to make sure the maximum intensity of D peak is approached. The annealing process for each graphene sample keeps at the same condition: annealing at 500 °C for 15 minutes and the vacuum level is 5×10<sup>-5</sup> mbar.

**Nudged elastic band simulations.** The energy barriers of edge closing of bilayer graphene, modeled as shown in Figure 2, have been studied with nudged elastic band method. First principles total energy calculations of DFT are performed within Perdew-Burke-Ernzerhof (PBE) generalized gradient approximation. The projected augmented wave method as implemented in the VASP code<sup>33–35</sup> is employed to solve the Kohn-Sham equations. A kinetic energy cutoff of 400 eV and the k-points sampling of 24×1×1 are used for simulating CEBGs. All model structures are optimized with the vacuum separation set to be more than 10 Å, and the total energy converges to 1 meV.

- Girit, C. O. *et al.* Graphene at the edge: stability and dynamics. *Science* **323**, 1705–1708, (2009).
- Liu, Z., Suenaga, K., Harris, P. J. F. & Iijima, S. Open and Closed Edges of Graphene Layers. *Phys. Rev. Lett.* **102**, 015501, (2009).
- Huang, J. Y. *et al.* In situ observation of graphene sublimation and multi-layer edge reconstructions. *Proc. Natl. Acad. Sci. U. S. A.* **106**, 10103–10108, (2009).
- Liu, L. *et al.* Graphene diode, with bandgap opened and charge separated by pseudospin interaction. *Nat. Commun.* **submitted**, NCOMMS-10-02179.
- Son, Y. W., Cohen, M. L. & Louie, S. G. Energy gaps in graphene nanoribbons. *Phys. Rev. Lett.* **97**, 216803, (2006).
- Kobayashi, Y., Fukui, K., Enoki, T. & Kusakabe, K. Edge state on hydrogen-terminated graphite edges investigated by scanning tunneling microscopy. *Phys. Rev. B* **73**, 125415, (2006).
- Pisani, L., Chan, J. A., Montanari, B. & Harrison, N. M. Electronic structure and magnetic properties of graphitic ribbons. *Phys. Rev. B* **75**, 064418, (2007).
- Cervantes-Sodi, F., Csanyi, G., Piscanec, S. & Ferrari, A. C. Edge-functionalized and substitutionally doped graphene nanoribbons: Electronic and spin properties. *Phys. Rev. B* **77**, 165427, (2008).
- Koskinen, P., Malola, S. & Hakkinen, H. Self-passivating edge reconstructions of graphene. *Phys. Rev. Lett.* **101**, 115502, (2008).
- Koskinen, P., Malola, S. & Hakkinen, H. Evidence for graphene edges beyond zigzag and armchair. *Phys. Rev. B* **80**, 073401, (2009).
- You, Y. M., Ni, Z. H., Yu, T. & Shen, Z. X. Edge chirality determination of graphene by Raman spectroscopy. *Appl. Phys. Lett.* **93**, 163112, (2008).
- Casiraghi, C. *et al.* Raman spectroscopy of graphene edges. *Nano Lett.* **9**, 1433–1441, (2009).
- Basko, D. M. Boundary problems for Dirac electrons and edge-assisted Raman scattering in graphene. *Phys. Rev. B* **79**, 205428, (2009).
- Gupta, A. K., Russin, T. J., Gutierrez, H. R. & Eklund, P. C. Probing graphene edges via Raman scattering. *ACS Nano* **3**, 45–52, (2009).
- Chuvilin, A., Kaiser, U., Bichoutskaia, E., Besley, N. A. & Khlobystov, A. N. Direct transformation of graphene to fullerene. *Nature Chem.* **2**, 450–453, (2010).
- Xu, Y. N. *et al.* Thermal dynamics of graphene edges investigated by polarized Raman spectroscopy. *ACS Nano* **5**, 147–152, (2011).
- Joly, V. L. J. *et al.* Observation of magnetic edge state in graphene nanoribbons. *Phys. Rev. B* **81**, 245428, (2010).
- Jia, X. T. *et al.* Controlled formation of sharp zigzag and armchair edges in graphitic nanoribbons. *Science* **323**, 1701–1705, (2009).
- Cruz-Silva, E. *et al.* Controlling edge morphology in graphene layers using electron irradiation: from sharp atomic edges to coalesced layers forming loops. *Phys. Rev. Lett.* **105**, 045501, (2010).
- Pimenta, M. A. *et al.* Studying disorder in graphite-based systems by Raman spectroscopy. *Phys. Chem. Chem. Phys.* **9**, 1276–1291, (2007).
- Chen, J. H., Cullen, W. G., Jang, C., Fuhrer, M. S. & Williams, E. D. Defect scattering in graphene. *Phys. Rev. Lett.* **102**, 236805, (2009).
- Ni, Z. H. *et al.* Uniaxial strain on graphene: Raman spectroscopy study and bandgap opening. *ACS Nano* **2**, 2301–2305, (2008).
- Ni, Z. H. *et al.* Probing charged impurities in suspended graphene using Raman spectroscopy. *ACS Nano* **3**, 569–574, (2009).
- Zhan, D. *et al.* FeCl<sub>3</sub>-based few-layer graphene intercalation compounds: single linear dispersion electronic band structure and strong charge transfer doping. *Adv. Funct. Mater.* **20**, 3504–3509, (2010).
- Cancado, L. G., Pimenta, M. A., Neves, B. R. A., Dantas, M. S. S. & Jorio, A. Influence of the atomic structure on the Raman spectra of graphite edges. *Phys. Rev. Lett.* **93**, 247401, (2004).
- Basko, D. M., Piscanec, S. & Ferrari, A. C. Electron-electron interactions and doping dependence of the two-phonon Raman intensity in graphene. *Phys. Rev. B* **80**, 165413, (2009).
- Gupta, A. K., Nisoli, C., Lammert, P. E., Crespi, V. H. & Eklund, P. C. Curvature-induced D-band Raman scattering in folded graphene. *J. Phys. Condens. Matter.* **22**, 334205, (2010).
- Feng, J., Qi, L., Huang, J. Y. & Li, J. Geometric and electronic structure of graphene bilayer edges. *Phys. Rev. B* **80**, 165407, (2009).
- Calizo, I., Bao, W. Z., Miao, F., Lau, C. N. & Balandin, A. A. The effect of substrates on the Raman spectrum of graphene: Graphene-on-sapphire and graphene-on-glass. *Appl. Phys. Lett.* **91**, 201904, (2007).
- Ni, Z. H. *et al.* Graphene thickness determination using reflection and contrast spectroscopy. *Nano Lett.* **7**, 2758–2763, (2007).
- Wang, Y. Y., Ni, Z. H., Shen, Z. X., Wang, H. M. & Wu, Y. H. Interference enhancement of Raman signal of graphene. *Appl. Phys. Lett.* **92**, 043121, (2008).
- Ghosh, S. *et al.* Dimensional crossover of thermal transport in few-layer graphene. *Nature Mater.* **9**, 555–558, (2010).
- Kresse, G. & Hafner, J. AB Initio molecular-dynamics for Liquid-metals. *Phys. Rev. B* **47**, 558–561, (1993).
- Kresse, G. & Hafner, J. AB Initio molecular dynamics for open-shell transition metals. *Phys. Rev. B* **48**, 13115–13118, (1993).
- Kresse, G. & Furthmüller, J. Efficiency of ab-initio total energy calculations for metals and semiconductors using a plane-wave basis set. *Comput. Mater. Sci.* **6**, 15–50, (1996).

## Author contributions

D.Z., Y.X., Z.N., C.Z., L.L. and Z.S. conceived and designed the experiments. Y.X. performed the experiments; J.Y. and L.L. performed the theoretical calculations. D.Z., Z.N. and L.L. collected and analysed the data. D.Z., Y.X., Z.N. L.L. and Z.S. co-wrote the paper. All authors discussed the results and commented on the manuscript.

## Additional information

**Competing financial interests:** The authors declare no competing financial interests.

**License:** This work is licensed under a Creative Commons Attribution-NonCommercial-ShareAlike 3.0 Unported License. To view a copy of this license, visit <http://creativecommons.org/licenses/by-nc-sa/3.0/>

**How to cite this article:** Zhan, D. *et al.* Low temperature edge dynamics of AB-stacked bilayer graphene: Naturally favored closed zigzag edges. *Sci. Rep.* **1**, 12; DOI:10.1038/srep00012 (2011).